

# Post-FEC BER Prediction for Bit-Interleaved Coded Modulation with Probabilistic Shaping

Tsuyoshi Yoshida, *Member, IEEE*, Alex Alvarado, *Senior Member, IEEE*,  
Magnus Karlsson, *Fellow, OSA; Senior Member, IEEE*, and Erik Agrell, *Fellow, IEEE*

**Abstract**—Accurate performance prediction after forward error correction (FEC) decoding is essential for system design in optical fiber communications. While generalized mutual information (GMI) has been shown to be successful for soft-decision decoded systems, for systems using probabilistic shaping (PS), GMI is less well correlated with the bit-error rate after soft-decision decoding. The proposed metrics for such systems are instead normalized GMI (NGMI) and asymmetric information (ASI). They are good to predict BER after FEC decoding or to give an FEC limit in bit-interleaved coded modulation (BICM) with PS, but their relation has not been clearly explained so far. In this paper, we show that NGMI and ASI are equal under matched decoding but not under mismatched decoding. We also examine pre-FEC BER and ASI/NGMI over Gaussian and nonlinear fiber-optic channels with approximately matched decoding. ASI/NGMI always shows better correlation with post-FEC BER than pre-FEC BER for BICM with PS. On the other hand, post-FEC BER can differ at a given ASI/NGMI when we change the bit mapping, which describes how each bit in a codeword is assigned to a bit tributary.

**Index Terms**—Bit error rate, bitwise decoding, bit-interleaved coded modulation, forward error correction, generalized mutual information, modulation, mutual information, optical fiber communication, probabilistic shaping.

## I. INTRODUCTION

In fiber-optic communications, forward error correction (FEC) is widely deployed due to the severe requirements of the residual bit error rate (BER) of the received data, which can be as low as  $< 10^{-15}$ . In research and system evaluations, actual encoding and decoding gives the most reliable performance

Manuscript received October 31, 2019.

This work was presented in part at the 2017 European Conference on Optical Communication [14]. It was supported in part by the Swedish Research Council (VR) under grant no. 2017-03702 and “Massively Parallel and Sliced Optical Network (MAPLE),” the Commissioned Research of National Institute of Information and Communications Technology (NICT), Japan (project number 20401). The work of A. Alvarado is supported by the Netherlands Organization for Scientific Research (NWO) via the VIDI Grant ICONIC (project number 15685) and has received funding from the European Research Council (ERC) under the European Union’s Horizon 2020 research and innovation programme (grant agreement No 757791).

T. Yoshida was a visiting researcher of the Fiber Optic Communications Research Center (FORCE), Chalmers University of Technology, SE-41296 Gothenburg, Sweden. He is with Information Technology R&D Center, Mitsubishi Electric Corporation, Kamakura, Kanagawa, 247-8501 Japan. Currently he also belongs to Graduate School of Engineering, Osaka University, Suita, Osaka, 505-0871 Japan (e-mail: Yoshida.Tsuyoshi@ah.MitsubishiElectric.co.jp).

A. Alvarado is with the Information and Communication Theory Lab, Signal Processing Systems Group, Department of Electrical Engineering, Eindhoven University of Technology, Eindhoven 5600 MB, The Netherlands.

M. Karlsson and E. Agrell are with Fiber Optic Communications Research Center (FORCE), Chalmers University of Technology, SE-41296 Gothenburg, Sweden.

assessment. However, it is less attractive because it requires significant efforts to examine very-low BERs and the results are specific to the examined FEC code. If one instead could quantify the performance and decouple the transmission and coding parts of the system it would greatly simplify system development and characterization. Historically, a so-called *FEC limit*, a certain value of the BER before the FEC decoder (hence referred to as pre-FEC BER), has been employed. It predicts the post-FEC (after decoder) performance, to quantify the real available data rates, and to measure margins in deployed systems. On the other hand, information-theoretic tools [1] have become increasingly common in fiber-optic communications after the emergence of coherent detection systems with digital signal processing (DSP). For example, transmission techniques are often evaluated using achievable information rates (AIRs), which give an indication of the potential data rate assuming ideal FEC performance. We should also consider the gap between the AIR and system throughput (sometimes called “information rate”) and how it is constrained by nonideal FEC performance [2]–[4]. Thus how information-theoretic metrics like AIR relate to the system throughput in practically relevant cases needs to be understood in detail.

This paper focuses on bit-interleaved coded modulation (BICM) [5]–[8] with binary soft-decision (SD) FEC, because it has been widely deployed due to its low implementation complexity and design simplicity. We combine BICM with *probabilistic shaping* (PS) with reverse concatenation of FEC and PS coding which shapes the modulation symbol amplitudes.<sup>1</sup> This is known as probabilistic amplitude shaping (PAS), and it can approach the Shannon capacity as shown in [9], [10].

Several reports predict the post-FEC BER by employing code-independent metrics. For BICM, an AIR is the so-called generalized mutual information (GMI) [8], and its normalized value, ranging from 0 to 1, has been shown to be a good predictor of post-FEC BER [11, Sec. IV]. In contrast, pre-FEC BER is not good for very low code rates, i.e., pre-FEC BER vs. post-FEC BER curves will differ significantly between low- and high-order modulation formats [11, Figs. 3(a), 8(a)]. An similar metric must be redefined for PAS due to the

<sup>1</sup>The PS coding was called “distribution matching (DM)” in the original PAS literature [9] and rephrased to “PS encoding/decoding” more recently in [10]. There are many PS coding techniques, e.g., DM with an explicit target probability distribution [23], [24]. Alternatively, one can use a DM without constant composition and any explicit target distribution, but where the distribution converges after averaging over time [19], [25]. In other works it is simply called shaping [26].

dependence between bit tributaries and the nonuniform symbol constellations. It has been found that a normalized GMI (NGMI), suitably extended to PAS [3], [12], or asymmetric information (ASI), defined from bit-weighted log-likelihood ratios [13], [14], are good predictor metrics for these systems. These metrics have been used in, e.g., [15], [16]. Both NGMI and ASI cover also the uniform (non-PS) BICM cases, which makes these metrics more general than the GMI.

There are three issues in the prior literature [3], [11]–[14], [17]–[19] that call for deeper studies related to these metrics. First, the sometimes subtle relationships between the used rates and metrics should be clarified. For example, the relationship between the (normalized) GMI [3], [11], [12] and ASI [13], [14], [18], [19] for PAS has not been sufficiently explained and clarified. Recently, these two metrics have been compared for the first time and found to differ [20]. The second issue is the lack of studies of the post-FEC performance prediction after nonlinear fiber-optic transmission for PAS. The third issue is that there are yet no investigations of the dependence of post-FEC BER on bit mapping. When several bits are mapped onto a modulated symbol, each bit tributary can have different pre-FEC performances. For example, the least significant bit has the worst performance in a regular binary reflected Gray-coded pulse amplitude modulated (PAM) signal. Thus, the post-FEC BER may differ depending on the bit mapping (how a bit in the FEC codeword is mapped to a bit tributary), even if the other conditions are the same, as implied in [9], [21]. More generally, the bit mapping dependence comes from the FEC code structure, so code-independent performance metrics cannot take it into account. Note that density evolution or exit chart analysis, which can take the code structure into account, would be useful in some cases though they are limited only to the specific code used.

This work extends our previous works [13], [14], where we examined the usefulness of ASI under fiber-optic channels under different nonlinear simulation conditions, by addressing the unsolved issues in the literature listed above. The novelties of this paper are

- a detailed analysis of the relations between performance metrics of NGMI and ASI, and
- investigation of performance metrics as post-FEC BER predictor with different bit mappings and various nonlinear transmission cases.

We stress that the above metrics relates to post-FEC BER. We do however recognize that the most relevant system output error rates are those after PS decoding in PAS systems, and that the PS decoding tends to increase BER, as shown in [18], [19], [22] (e.g., 5 to 200 times [19, Fig. 4] and 10 to 50 times [22, Fig. 12]). The relationship between BERs before and after PS decoding depends on the specific cross layout of FEC and PS codes [19, Figs. 3]. Since the BER after PS decoding can be estimated from the post-FEC BER [19, Sec. VII], this paper, in the interest of generality, focuses only on performance metrics before FEC decoding that estimates the post-FEC BER.

The rest of the paper is organized as follows. Relevant metrics are summarized in Sec. II, where the equivalence between NGMI and ASI is discussed in detail. Bit mapping dependence and prediction performance over the nonlinear

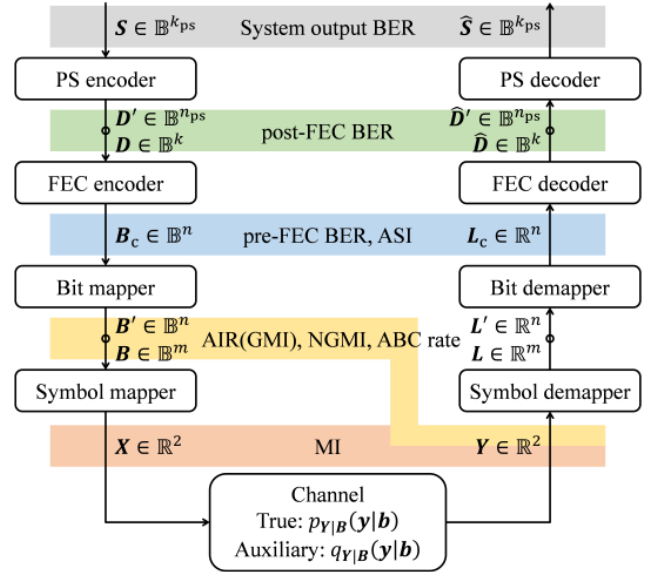


Fig. 1. System model of BICM with PS. Here we show the notations of the signals with the number of the dimensions and key performance metrics that will be discussed in this paper. The channel is assumed (or approximated) to be discrete and memoryless.

fiber-optic channel are shown in Secs. III and IV, resp. Sec. V concludes the paper.

## II. THEORY FOR RELEVANT RATES AND METRICS

In this section, after definition of the system model (Sec. II-A), we review achievable rates (Sec. II-B) and relevant performance metrics before and after FEC decoding (Sec. II-C). Then the relation of information rate and FEC code rate is explained (Sec. II-D), which is useful for understanding the metrics. Finally we discuss the equivalence of the NGMI and ASI (Sec. II-E).

### A. System model

We consider the system model shown in Fig. 1. At the transmitter, the source bits  $S \in \mathcal{B}^{k_{ps}}$  are assumed to be uniformly distributed and independent. The source bits are converted to the shaped bits  $D' \in \mathbb{B}^{n_{ps}}$  by the PS encoder based on PAS<sup>2</sup>, where  $\mathbb{B} = \{0, 1\}$  and  $(n_{ps}, k_{ps})$  are the numbers of PS encoder output and input bits per PS codeword. A circle in Fig. 1 denotes block length conversion, e.g.,  $\mathbb{B}^{n_{ps}}$  to  $\mathbb{B}^k$ . A systematic FEC encoding is applied to the payload bits  $D \in \mathbb{B}^k$  for PAS, whereby the encoded bits  $B_c \in \mathbb{B}^n$  are generated, where  $(n, k)$  are the FEC codeword length and number of information bits per FEC codeword. The bits  $B_c$  are then mapped to bit tributaries in  $B' \in \mathbb{B}^{m \cdot (n/m)}$ , where  $m$  denotes the number of bit tributaries conveyed by each two-dimensional symbol. Next the bits  $B \in \mathbb{B}^m$  are mapped into a two-dimensional symbol  $X \in \mathbb{R}^2$ , where  $\mathbb{R}$  denotes the set of real numbers. For simplicity,  $n/m$  is assumed to be an integer. After being transmitted over the channel

<sup>2</sup>In this work we focus on PAS, though reverse concatenation PS is more general, e.g., it can comprise different coding/shaping schemes like multi-level coding. PAS shapes absolute amplitudes only in each dimension and does not shape sign bits [9].

(assumed/approximated to be discrete and memoryless), the received symbol  $\mathbf{Y} \in \mathbb{R}^2$  is demapped to bitwise *a posteriori* L-values, also known as log-likelihood ratios  $\mathbf{L} \in \mathbb{R}^m$ .

The L-values  $\mathbf{L}' \in \mathbb{R}^{m \cdot (n/m)}$  are bit-demapped to  $\mathbf{L}_c \in \mathbb{R}^n$ , which are decoded to  $\hat{\mathbf{D}} \in \mathbb{B}^k$  to recover the shaped bits. The PS decoding is performed on  $\hat{\mathbf{D}}' \in \mathbb{B}^{n_{ps}}$  when PAS is employed. Finally the source bits are recovered as  $\hat{\mathbf{S}} \in \mathbb{B}^{k_{ps}}$ . For uniform signaling  $\mathbf{D} = \mathbf{S}$  and  $\hat{\mathbf{S}} = \hat{\mathbf{D}}$ .

The L-value is calculated per bit tributary  $i$  from the received symbol  $Y$ . The *a posteriori* L-value  $L_i(\mathbf{Y})$  is defined as [8, Eqs. (3.31)–(3.32), (3.39)]

$$L_i(\mathbf{y}) \triangleq L_i^{(\text{apr})} + L_i^{(\text{ex})}(\mathbf{y}). \quad (1)$$

Here,  $L_i^{(\text{apr})}$  and  $L_i^{(\text{ex})}$  are *a priori* and *extrinsic* L-values, i.e.,

$$L_i^{(\text{apr})} \triangleq \ln \frac{P_{B_i}(0)}{P_{B_i}(1)}, \quad (2)$$

$$L_i^{(\text{ex})}(\mathbf{y}) \triangleq \ln \frac{q_{\mathbf{Y}|B_i}(\mathbf{y}|0)}{q_{\mathbf{Y}|B_i}(\mathbf{y}|1)}, \quad (3)$$

$$L_i(\mathbf{y}) = \ln \frac{q_{B_i, \mathbf{Y}}(0, \mathbf{y})}{q_{B_i, \mathbf{Y}}(1, \mathbf{y})}, \quad (4)$$

where  $B_i$  and  $P_{B_i}(b)$  denote bits for bit tributary index  $i$  and the probability of bits  $B_i$  being  $b \in \mathbb{B}$ . The notations  $q_{B_i, \mathbf{Y}}(b, \mathbf{y})$  and  $q_{\mathbf{Y}|B_i}(\mathbf{y} | b)$  are the joint and conditional distributions assumed in the demapper, resp., of  $\mathbf{Y}$  and  $B_i$ . We note here that in general the “auxiliary channel”  $q_{\mathbf{Y}|B_i}(\mathbf{y} | b)$  is different from the true channel  $p_{\mathbf{Y}|B_i}(\mathbf{y} | b)$  (see Fig. 1). The  $L_i(\mathbf{Y})$  is bit demapped and fed to the FEC decoder.

In the BICM scheme, the bit mapper/demapper in Fig. 1 is usually described as bit interleaver/de-interleaver. The bit interleaver shuffles the bit positions [8, Sec. 2.7] and determines the bit tributary  $i$  for each bit. An important motivation for the shuffling is to scatter burst errors caused by the channel, or by an inner decoder (if there is one). In this work we mainly focus on how a bit in the FEC codeword is assigned to a bit tributary in the symbol, which is independent of burst errors.

## B. Achievable rates

While an AIR of a symbol-wise receiver is mutual information (MI)  $I(\mathbf{X}; \mathbf{Y})$ , that of a bit-wise receiver is GMI [8, Eqs. (4.34), (4.35)]. It is defined for any memoryless channel as

$$\text{GMI} \triangleq \max_{s \geq 0} I_{q, s}^{\text{gmi}}(\mathbf{B}; \mathbf{Y}), \quad (5)$$

$$I_{q, s}^{\text{gmi}}(\mathbf{B}; \mathbf{Y}) \triangleq \mathbb{E}_{\mathbf{B}, \mathbf{Y}} \left[ \log_2 \frac{q(\mathbf{B}, \mathbf{Y})^s}{\sum_{b \in \mathbb{B}^m} P_{\mathbf{B}}(b) q(b, \mathbf{Y})^s} \right], \quad (6)$$

where  $\mathbb{E}_{\mathbf{B}, \mathbf{Y}}[\cdot]$  denotes the expectation under the joint probability  $p_{\mathbf{B}, \mathbf{Y}}(\mathbf{b}, \mathbf{y})$ , and  $q(\mathbf{b}, \mathbf{y})$  denotes an arbitrary symbol decoding metric. In (6) the parameter  $s$  can be interpreted as a parameter that controls the auxiliary channel  $q$ . This optimization parameter can also be connected to correcting mismatched L-values, as done in [8, Ch. 7], [27]–[29]. Under matched decoding (i.e.,  $q_{\mathbf{Y}|B}(\mathbf{y} | b) = p_{\mathbf{Y}|B}(\mathbf{y} | b)$ ),  $s = 1$ .

When we employ bit metric decoding (BMD), the symbol decoding metric becomes [30, Eq. (22)]

$$q(\mathbf{b}, \mathbf{y}) = \frac{\prod_{i=1}^m P_{B_i}(b)}{P_{\mathbf{B}}(\mathbf{b})} \prod_{i=1}^m q_{\mathbf{Y}|B_i}(\mathbf{y} | b). \quad (7)$$

The bit decoding metric  $q_{\mathbf{Y}|B_i}(\mathbf{y} | b)$  is given by the auxiliary channel assumed in the demapper  $q_{\mathbf{Y}|B}(\mathbf{y} | \mathbf{b})$  as [30, Eq. (11)]

$$q_{\mathbf{Y}|B_i}(\mathbf{y} | b) = \frac{1}{P_{B_i}(b)} \sum_{\mathbf{b} \in \mathbb{B}^m: b_i = b} P_{\mathbf{B}}(\mathbf{b}) q_{\mathbf{Y}|B}(\mathbf{y} | \mathbf{b}). \quad (8)$$

When PAS is added to BICM, an AIR is the BMD rate [17, Eq. (51)]

$$R_{\text{bmd}} \triangleq \left[ \mathbb{H}(\mathbf{B}) - \sum_{i=1}^m \mathbb{H}(B_i | \mathbf{Y}) \right]^+. \quad (9)$$

In (9)  $\mathbb{H}(\cdot)$ ,  $\mathbb{H}(\cdot | \cdot)$ , and  $[\cdot]^+$  denote entropy, conditional entropy, and  $\max\{\cdot, 0\}$ , resp. While the operation  $[\cdot]^+$  prevents  $R_{\text{bmd}}$  from being negative, the net difference without  $[\cdot]^+$ ,

$$\Delta_{\mathbb{H}} \triangleq \mathbb{H}(\mathbf{B}) - \sum_{i=1}^m \mathbb{H}(B_i | \mathbf{Y}) \quad (10)$$

will also be useful in the analysis.

In [3, Eqs. (12), (13), Appendix], there is no  $\max_{s \geq 0}(\cdot)$  operation in the definition of GMI (5), so  $s = 1$  is implicitly assumed. In that case,

$$\text{GMI} = \Delta_{\mathbb{H}}. \quad (11)$$

as derived in [3].

## C. Performance metrics

A common performance target in deployable systems is that the post-FEC BER,

$$\text{BER}_{\text{post}} \triangleq \sum_{b \in \mathbb{B}} P_{D, \hat{D}}(b, 1 - b), \quad (12)$$

must be almost error-free, i.e.,  $\text{BER}_{\text{post}} < 10^{-15}$ . To evaluate if the obtained performance corresponds to error-free operation, so-called *FEC limits* have been utilized. This concept relies on the assumption that there exists a one-to-one mapping between the post-FEC BER and certain metrics before FEC decoding. If true it would enable accurate performance estimations in experiments or simulations without implementing FEC. The most common metric has been the BER before FEC decoding, pre-FEC BER, defined as

$$\text{BER}_{\text{pre}} \triangleq \sum_{b \in \mathbb{B}} P_{B, \text{sign}(L)}(b, 1 - b), \quad (13)$$

where  $L \in \mathbb{R}$  (without the index  $i$ ) denotes “mixed” L-value in an FEC codeword. The variable  $L$  therefore denotes an element of the L-value vector before FEC decoding,  $\mathbf{L}_c \in \mathbb{R}^n$ . Historically, this metric was used for hard-decision (HD) FEC, and it is accurate for memoryless HD systems. However, its accuracy is not enough for SD-FEC, particularly at lower code rates [11, Fig. 3(a), 8(a)], [31, Fig. 3]. Instead,  $\text{GMI}/m$  was

introduced and worked well for uniform signaling with SD-FEC.<sup>3</sup> Its value range is limited to  $[0,1]$  for uniform signaling. To extend this to the PAS case, normalization of the BMD rate  $R_{\text{bmd}}$  by its maximum value  $\mathbb{H}(\mathbf{B})$  was introduced as the normalized AIR [13, Eq. (7)]

$$\text{Normalized AIR} \triangleq R_{\text{bmd}}/\mathbb{H}(\mathbf{B}). \quad (14)$$

The normalized AIR in (14) does not work for PAS, as shown in [13].

Instead of the simple normalization in (14), a useful metric is

$$\text{NGMI} \triangleq 1 - (\mathbb{H}(\mathbf{B}) - \text{GMI})/m, \quad (15)$$

$$= 1 - \left( \mathbb{H}(\mathbf{B}) - \max_{s \geq 0} I_{q,s}^{\text{gmi}}(\mathbf{B}; \mathbf{Y}) \right) / m. \quad (16)$$

The NGMI was first studied in [31] for uniform signals and later extended to PS in [12], [3, Eq. (15)].<sup>4</sup> In (16), we generalize the concept further by including the optimization over  $s$ , which is important for mismatched decoding. The NGMI in (16) with  $s = 1$  can be shown to be the same as the *achievable binary code rate* (ABC rate) defined in [17, Example 4.1]

$$\text{NGMI} = \text{ABC rate} \triangleq 1 - \frac{1}{m} \sum_{i=1}^m \mathbb{H}(B_i | \mathbf{Y}). \quad (17)$$

In other words, the NGMI in (16) coincides with the ABC rate when the auxiliary channel is matched to the true channel ( $q_{\mathbf{Y}|B_i}(\mathbf{y} | b) = p_{\mathbf{Y}|B_i}(\mathbf{y} | b)$ , and thus,  $s = 1$ ). The ABC rate is therefore a special case of the NGMI, and thus, from now on we will not discuss the ABC rate any further.

The NGMI gives the maximum FEC code rate for error-free operation with an ideal FEC in the PAS scheme, as explained in [13, Sec. III], [3, Sec. IV], and also in Sec. II-D in this paper.

Independently of the NGMI, the *asymmetric information* (ASI) was introduced in [13] as

$$\text{ASI} \triangleq 1 - \mathbb{h}(L_a | |L_a|) = 1 + \mathbb{h}(|L_a|) - \mathbb{h}(L_a), \quad (18)$$

where  $\mathbb{h}(\cdot | \cdot)$  and  $\mathbb{h}(\cdot)$  denote conditional differential entropy and differential entropy, resp. The *asymmetric L-value*  $L_a$  and its probability density function (pdf) are given by

$$L_a \triangleq (-1)^b L, \quad (19)$$

where  $b$  is the transmitted bit, and

$$q_{L_a}(l) = \sum_{b \in \mathbb{B}} P_B(b) q_{L|B}((-1)^b \cdot l | b). \quad (20)$$

Fig. 2 shows an example of the pdfs for PAS 64-ary quadrature amplitude modulation (64-QAM), a shaping scheme that will be explained in Sec. III. Fig. 2(a) shows the joint distribution  $q_{B,L}(b, l)$  and Fig. 2(b) the pdfs of the ‘‘symmetrized’’ L-values  $q_{B,L}(0, l)$ ,  $q_{B,L}(1, -l)$ , and  $q_{L_a}(l)$  [33]. The pdfs are asymmetric. We showed in [13], [14] that the ASI predicts the post-FEC BER well for both uniform and shaped signaling.

<sup>3</sup>If there are burst errors and the FEC codeword length is limited, interleaving over time is required to disperse the errors. If not, the post-FEC BER will be degraded compared with the expectation. More details are given in [32, Sec. II-B].

<sup>4</sup>Here (10) and (11) are applied to (15). In the regime  $\Delta_{\mathbb{H}} \geq 0$ ,  $\text{NGMI} = 1 - (\mathbb{H}(\mathbf{B}) - R_{\text{bmd}})/m$ .

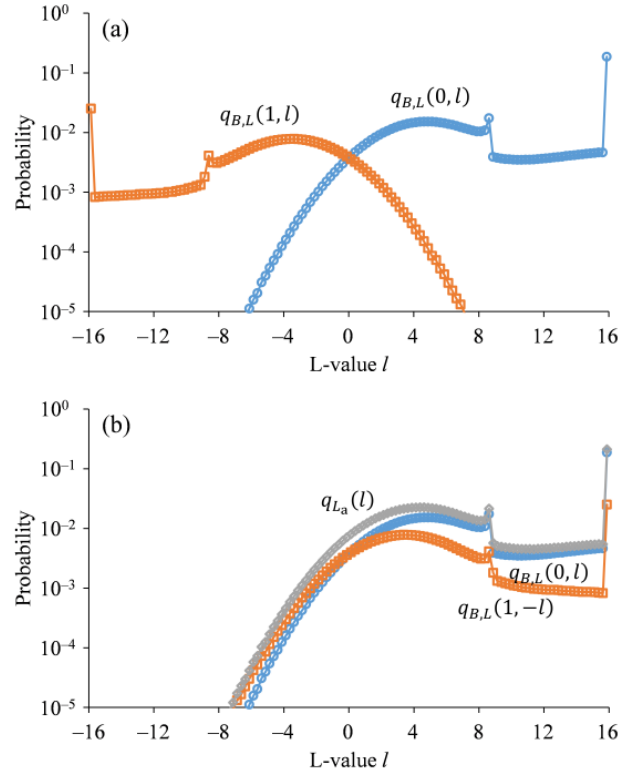


Fig. 2. An example of pdfs in the case of PAS-64-QAM (system (i) in Tab. II) at a SNR of 9 dB: (a)  $q_{B,L}(b, l)$  and (b)  $q_{L_a}(l)$ . The high peaks are due to clipping the pdf by a finite range histogram. The effect of the clipping at large  $L_a$  in (b) is negligible for calculating the ASI.

#### D. Information rate and code rate with rate loss

The system throughput (without any overhead) is characterized not only by the AIR, but also by the rate loss due to nonideal FEC<sup>5</sup> and PS coding.<sup>6</sup> The information rate  $R$ , which is the AIR minus FEC and PS coding rate losses, can be written as

$$R \triangleq \mathbb{H}(\mathbf{B}) - R_{\text{loss}} - (1 - R_c)m, \quad (21)$$

where  $R_c = k/n$  is the FEC code rate, and  $R_{\text{loss}}$  denotes the PS coding rate loss [9, Sec. V-B], [24, Eq. (4)]. Note that here we define it per two dimensions, as also done in [19, Eq. (3)]. Example values of  $\mathbb{H}(\mathbf{B})$ , and  $R_{\text{loss}}$  can be found in Sec. III-B, Tab. II. The AIR given by the BMD rate (9) is also corrected with the PS coding rate loss to [24, Eq. (15)]

$$\begin{aligned} R'_{\text{bmd}} &= \Delta_{\mathbb{H}} - R_{\text{loss}} \\ &= \mathbb{H}(\mathbf{B}) - \sum_{i=1}^m \mathbb{H}(B_i | \mathbf{Y}) - R_{\text{loss}} \end{aligned} \quad (22)$$

in the regime where  $\Delta_{\mathbb{H}} \geq 0$ . The information rate  $R$  in (21) must satisfy  $R \leq R'_{\text{bmd}}$ , where  $R'_{\text{bmd}}$  is given by (22). Hence, the FEC code rate satisfies

$$R_c \leq 1 - (\mathbb{H}(\mathbf{B}) - R_{\text{loss}} - R'_{\text{bmd}})/m. \quad (23)$$

The right-hand side of (23) is equal to the NGMI in (17).

<sup>5</sup>The difference between NGMI or ASI and the FEC code rate  $R_c$  is called coding gap in [3, Sec. IV]. It was considered also in [4], [34, Tab. II].

<sup>6</sup>Overheads for framing and pilot signals should be also accounted for in practice.

### E. Equivalence of NGMI and ASI

Here we explain the equivalence of NGMI in (15) and ASI in (18).

*Theorem 1:* When the auxiliary channel is any (*matched* or *mismatched*) discrete memoryless channel under BMD,

$$\text{ASI} = 1 - \left( \mathbb{H}(\mathbf{B}) - I_{q,s=1}^{\text{gmi}}(\mathbf{B}; \mathbf{Y}) \right) / m. \quad (24)$$

*Proof:* See Appendix A.  $\square$

*Theorem 2:* When the auxiliary channel is *mismatched* to the true (approximated) discrete memoryless channel under BMD (i.e.,  $q_{\mathbf{Y}|\mathbf{B}}(\mathbf{y}|\mathbf{b}) \neq p_{\mathbf{Y}|\mathbf{B}}(\mathbf{y}|\mathbf{b})$ ),

$$\text{ASI} \leq \text{NGMI}. \quad (25)$$

*Proof:* The optimum  $s$  may be  $\neq 1$  in (5), so the NGMI in (16) is larger than or equal to the ASI in (24) because  $\max_{s \geq 0} I_{q,s}(\mathbf{B}; \mathbf{Y}) \geq I_{q,s=1}(\mathbf{B}; \mathbf{Y})$ .  $\square$

*Theorem 3:* When the auxiliary channel is *matched* to the true (approximated) discrete memoryless channel under BMD (i.e.,  $q_{\mathbf{Y}|\mathbf{B}}(\mathbf{y}|\mathbf{b}) = p_{\mathbf{Y}|\mathbf{B}}(\mathbf{y}|\mathbf{b})$  and thus  $s = 1$  in (5)), and  $\Delta_{\mathbb{H}} \geq 0$ ,

$$\text{NGMI} = \text{ASI} = 1 - \mathbb{E}_{L_a} [\log_2(1 + \exp(-l))]. \quad (26)$$

*Proof:* By employing [8, Eq. (4.81)], the NGMI in (17) can be rewritten as (39).  $\square$

In research works for optical fiber communications under the discrete memoryless channel approximation, the auxiliary channel can be very close to the true (approximated) channel. Thus we will see almost matched decoding and the optimum  $s = 1$  in (5). As shown in Theorem 3, the NGMI and ASI coincide. On the other hand, if *a posteriori* L-values are derived with nonideal assumptions, we will see mismatched decoding and the optimum  $s$  may be  $\neq 1$  (Theorem 2). We note that the inequality  $\max_{s \geq 0} I_{q,s}(\mathbf{B}; \mathbf{Y}) \geq I_{q,s=1}(\mathbf{B}; \mathbf{Y})$  we used in the proof of Theorem 2 could be a possible reason why smaller ASI than NGMI were observed in [20, Fig. 1]. A typical mismatched decoding case will be at live traffic transmissions with system margins of several dB. The demapper in realtime DSP will be assume a fixed SNR optimized to the FEC limit because the system should be resilient to sudden performance degradations even if there is a margin. Then the auxiliary and true channels can be mismatched by several dBs, and the true performance before FEC decoding is characterized by the ASI, which takes mismatched L-values derivation into account. We keep the analysis of the difference between the NGMI and ASI under such situation as a future work. As for the simulations in this work, we will derive matched *a posteriori* L-values (so optimum  $s = 1$ ) in the following sections. This assumption is reasonable because in the following simulations we will compare the performance around the FEC limit, in which case we will see almost matched decoding (and thus  $\text{NGMI} \approx \text{ASI}$ ). In the rest of the paper we thus study performance under conditions where ASI and NGMI are effectively equivalent, except where explicitly stated.

### III. PREDICTION IN VARIOUS BIT MAPPING AND MODULATION/SHAPING CASES

While quaternary phase-shift keying (QPSK) has only a single bit per in-phase and quadrature component, high-order QAM has several. Therefore, an asymmetric L-value combination over bits for the codeword space, i.e.,  $[L_{a,1}, L_{a,2}, \dots, L_{a,n}]$  where  $n$  denotes the FEC codeword length, becomes strongly dependent on the bit mapping for high-order QAM. The post-FEC decoding performance depends on the asymmetric L-value combination. The dependence is stronger in the case of a structured FEC code with a low code rate.

The bit mapping over the codeword should be optimized for the used FEC, modulation, and shaping. In case of low-rate FEC for uniform signaling, the bit mapping affects the post-FEC BER even if the other conditions are the same [21], [31, Fig. 5]. Examples of good bit mappings for PAS were reported in [9, Tab. V].

#### A. Considered bit mappings

To estimate the information-theoretic quantities in Sec. II, Monte-Carlo integration is a useful way to approximate an integration by a finite sum. If  $\mathbf{B}$  is represented by a sequence  $\beta[j]$  and  $\mathbf{L}$  by a sequence  $\lambda[j]$  for  $j = 1, \dots, mn_s$ , where  $n_s$  is the number of simulated symbols, then the symmetrized L-value sequence is calculated as  $\lambda_s[j] = (-1)^{\beta[j]} \lambda[j]$  according to (19). Then the ASI (26), (37) can be estimated as

$$\text{ASI} \approx 1 - \frac{1}{mn_s} \sum_{j=1}^{mn_s} \log_2(1 + \exp(-\lambda_s[j])). \quad (27)$$

While the same expression is found in [8, Ths. 4.20, 4.21], [11] for uniform signaling, it is valid for PAS, too, because the ASI works for both schemes as explained in Sec. II-D.<sup>7</sup>

Tab. I shows the examined bit mappings. A bit mapping is denoted as  $\mathbb{M} = [M_1, M_2, \dots, M_n]$  for the bit indexes 1 to  $n$  over the codeword, where each integer  $1, \dots, \bar{m}$  must occur  $n/\bar{m}$  times in  $\mathbb{M}$ . Note that  $\bar{m} = m/2$ , i.e., the number of bits per PAM symbol for square QAM, and that  $\bar{m} = m$  for cross QAM. To generate a square QAM symbol, two PAM symbols are combined. We consider the following three types of mappings.

- *Fixed structured bit mapping:* used for short-period structured bit mappings;  $\mathbb{M}_{\text{FS1}}$  and  $\mathbb{M}_{\text{FS2}}$  in Tab. I. These bit mappings are practically implementable in today's DSP.
- *Random bit mapping:* random permutation of bit position in a codeword by a random number, whose seed is changed at each codeword;  $\mathbb{M}_{\text{R}}$  in Tab. I. This is used only for benchmark purposes.
- *Fixed unstructured bit mapping:* random permutation of bit position in a codeword by a random number, whose seed is fixed;  $\mathbb{M}_{\text{FU}}$  in Tab. I. This is more practical than random bit mapping.

The first  $k$  and the last  $n - k$  components of  $\mathbb{M}$  denote the bit tributaries of the information bits and parity bits, resp.

<sup>7</sup>We believe that (27) is often used as NGMI in the optical fiber communication field because of its simplicity. Alternatively, one can estimate the ASI by approximating the pdf:s with a discrete histogram.

TABLE I

EXAMINED FIXED STRUCTURED ( $\mathbb{M}_{\text{FS1}}$  AND  $\mathbb{M}_{\text{FS2}}$ ), RANDOM ( $\mathbb{M}_{\text{R}}$ ), AND FIXED UNSTRUCTURED ( $\mathbb{M}_{\text{FU}}$ ) BIT MAPPINGS.  $\mathbf{R}(\mathbb{M}, s_{\text{R}})$  DENOTES A RANDOM PERMUTATION OF THE VECTOR  $\mathbb{M}$  WITH THE SEED  $s_{\text{R}}$ .  $\mathbb{M}^{\text{L}}$  DENOTES THE FIRST  $n - n/\bar{m}$  COMPONENTS OF  $\mathbb{M}$ .

Notation	Bit mapping
$\mathbb{M}_{\text{FS1}}$	$[\bar{m}, \dots, \bar{m}, \bar{m} - 1, \dots, \bar{m} - 1, \dots, 1, \dots, 1]$
$\mathbb{M}_{\text{FS2}}$	$[\bar{m}, \bar{m} - 1, \dots, 2, \dots, \bar{m}, \bar{m} - 1, \dots, 2, 1, \dots, 1]$
$\mathbb{M}_{\text{R}}$	$[\mathbf{R}(\mathbb{M}_{\text{FS1}}^{\text{L}}), \text{random}], 1, \dots, 1]$
$\mathbb{M}_{\text{FU}}$	$[\mathbf{R}(\mathbb{M}_{\text{FS1}}^{\text{L}}), 1], 1, \dots, 1]$

For square QAM, the bit tributaries of the corresponding one-dimensional symbol are shown, e.g., three bit tributaries for 64-QAM. Bit tributary 1 determines the sign of the one-dimensional symbol, and bit tributaries 2 and 3 determines the absolute amplitude of the one-dimensional symbol. Usually we cannot control the distribution of parity bits, which are uniformly distributed. Thus not to change the probability mass function of PAS, we assign bit tributary 1 to the last  $n/\bar{m}$  components in all considered bit mappings, where  $n - k$  must be  $\leq n/\bar{m}$  for PAS.<sup>8</sup>

We employ the DVB-S2 low-density parity check (LDPC) code [35] as an SD-FEC, whose FEC codeword length  $n$  is 64800, and the number of decoding iterations was 50. The soft-demapping output is floating-point, and the decoding is done by floating-point operations with belief propagation. We assume the use of an outer HD-FEC to clean up the residual errors, having a code rate of 0.9922 and an input BER threshold of  $5 \times 10^{-5}$  [36] for error-free operation.<sup>9</sup> In Fig. 1, the FEC encoder includes an outer systematic HD-FEC encoder, a time interleaver, and an SD-FEC encoder, with the reverse operations on the receiver side. Here we assume a sufficiently long temporal interleaving and no residual burst errors after the SD-FEC decoder (the same assumption is found in [32, Sec. II-B]). If the interleaving length is insufficient, an error floor would result after HD-FEC decoding. The total FEC code rate is slightly smaller than that of the SD-FEC.

### B. Simulation results over the Gaussian channel under matched decoding

Fig. 3 shows the ASI from (27) for various modulation and shaping parameters as a function of SNR for the Gaussian channel under matched decoding, for which the ASI equals the NGMI as shown in Sec. II-E. Various modulation formats are examined and the parameters of PAS-64-QAM are shown in Tab. II. The PAS scheme requires a code rate<sup>10</sup>  $R_{\text{c}} \geq (m - 2)/m$ , so here the SD-FEC code rate  $R_{\text{sdc}}$  is set to 5/6 and bit mapping was set to  $\mathbb{M}_{\text{FS1}}$ . To generate PAS-64-QAM signals, constant composition distribution matching [23] was employed as the PS encoding with the PS codeword length of 1024 PAM symbols (512 QAM symbols). The

<sup>8</sup>Not all bits in bit tributary 1 are assigned to parity bits in the case of  $n - k < n/\bar{m}$ , but all bits in bit tributary 1 are placed in the last  $n/\bar{m}$  components for simplicity.

<sup>9</sup>The HD-FEC threshold is shown as the dashed line in the figures of post-FEC BER simulations.

<sup>10</sup>Note that  $m$  is defined as a two dimensional symbol in Sec. II-A, so there are two sign bits.

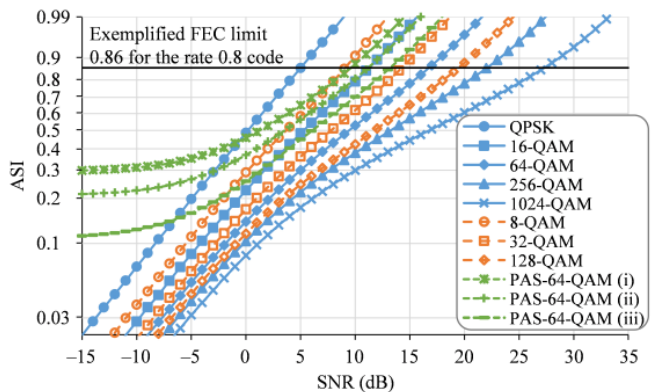


Fig. 3. ASI as a function of SNR. The vertical axis is scaled according to  $\log_{10}(-\log_{10}(1 - \text{ASI}))$  to make the QPSK-curve nearly linear. An alternative way to realize this linearization would be to plot  $J^{-1}(\text{ASI})$ , where  $J(\cdot)$  denotes the J-function, used in [37, Appendix].

TABLE II  
ONE-DIMENSIONAL PROBABILITY MASS FUNCTION OF PAS-64-QAM, AND TWO-DIMENSIONAL ENTROPIES AND PS RATE LOSS FOR SIMULATIONS.

Parameters	Uniform	PAS (i)	PAS (ii)	PAS (iii)
$P_{ X }(1)$	0.250	0.698	0.611	0.494
$P_{ X }(3)$	0.250	0.263	0.304	0.325
$P_{ X }(5)$	0.250	0.037	0.075	0.141
$P_{ X }(7)$	0.250	0.002	0.009	0.040
$\sum_{i=1}^m \mathbb{H}(B_i)$	6	4.238	4.754	5.356
$\mathbb{H}(\mathbf{B})$	6	4.124	4.604	5.226
$R_{\text{loss}}$	0	0.022	0.026	0.026

performance metrics before FEC decoding does not depend on the bit mapping ( $\mathbb{M}_{\text{FS1}}$ ,  $\mathbb{M}_{\text{FS2}}$ ,  $\mathbb{M}_{\text{R}}$ , or  $\mathbb{M}_{\text{FU}}$ ) in this simulation. The required SNR at a given target ASI can be obtained from the plot, assuming no bit mapping dependence. For example, considering the nonideal performance of FEC, a suitable ASI is 0.86 for  $R_{\text{c}} = 0.8$  [34, Tab. II] (see also footnote 5). The ASI for PAS shows a floor and does not approach zero at SNR:s  $< -15$  dB because of the nonuniformity. Note that no PAS-64-QAM system is available for reliable communications in this low-SNR regime, because the FEC code rate cannot be equal to the ASI or lower without violating the constraint  $R_{\text{c}} \geq (m - 2)/m$ .

Figs. 4 and 5 summarize the post-SD-FEC BER  $\text{BER}_{\text{post-SD}}$ , i.e., the BER after SD-FEC decoding, as a function of the pre-FEC BER defined in (13), and ASI). The modulation formats are Gray-coded QPSK, 16-QAM, 64-QAM, 256-QAM, and 1024-QAM, star-8-QAM labeled as in Tab. III, and PAS-64-QAM (i) in Tab. II. The SD-FEC code rates  $R_{\text{sdc}}$  are 1/3, 2/3, and 5/6 uniform QAM and 2/3 and 5/6 for the PAS.

In the case of fixed structured bit mappings in Fig. 4, the post-SD-FEC BER of the signal with high-order modulation and low code rates strongly depends on the bit mapping. This dependence comes from the structure of the code, so this is a limitation of using code-independent performance metrics. The bit mapping  $\mathbb{M}_{\text{FS2}}$  shows better post-FEC BER prediction performance than  $\mathbb{M}_{\text{FS1}}$  based on the ASI, while predictions based on the pre-FEC BER are inaccurate at the FEC code rate  $R_{\text{sdc}} = 1/3$  for both mappings. The BER prediction can fail if the fixed structured bit mapping is not tailored for the code,

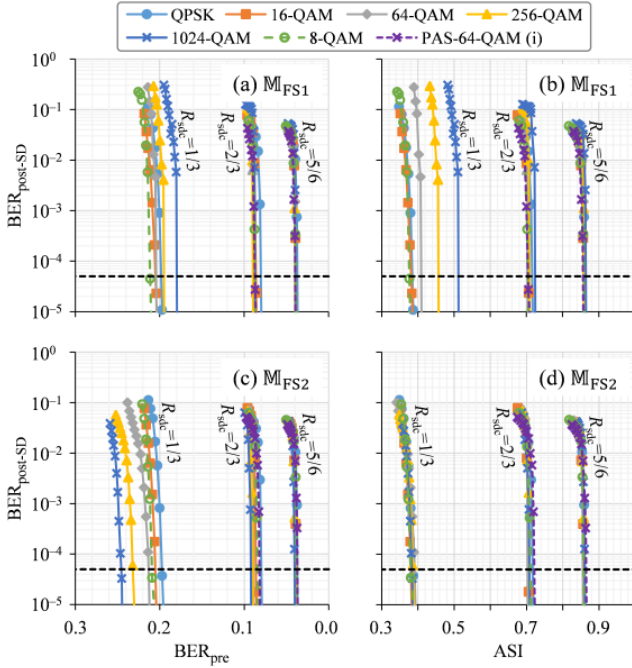


Fig. 4. Post-SD-FEC BER with fixed structured bit mappings. (a) and (b) are with  $\mathbb{M}_{\text{FS1}}$ . (c) and (d) are with  $\mathbb{M}_{\text{FS2}}$ . The dependence on pre-FEC BER is shown in (a) and (c), and on ASI in (b) and (d).

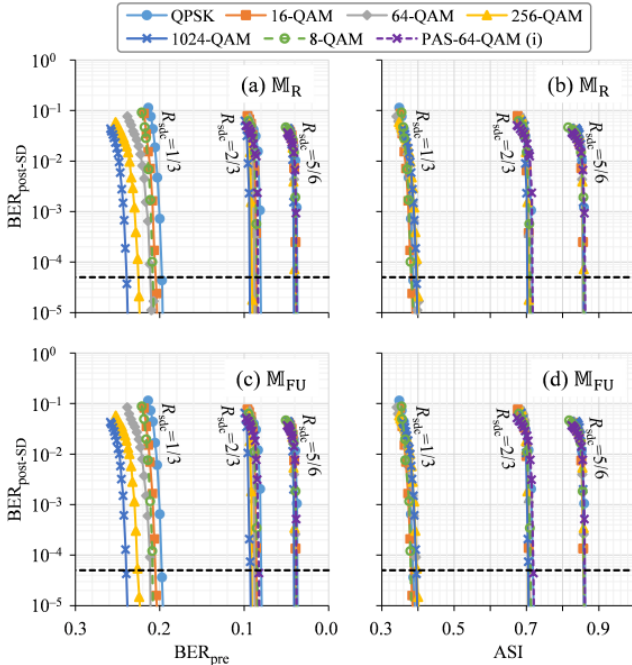


Fig. 5. Post-SD-FEC BER with random ( $\mathbb{M}_{\text{R}}$ ) or fixed unstructured ( $\mathbb{M}_{\text{FU}}$ ) bit mappings. (a) and (b) are with  $\mathbb{M}_{\text{R}}$ . (c) and (d) are with  $\mathbb{M}_{\text{FU}}$ . The dependence on pre-FEC BER is shown in (a) and (c), and on ASI in (b) and (d).

so the post-FEC BER does indeed depend on the combination of the FEC code structure and bit mapping.

As for the post-SD-FEC BER curves with random bit mapping  $\mathbb{M}_{\text{R}}$ , shown in the upper side of Fig. 5, ASI is clearly a better metric than pre-FEC BER because the convergence of the curves is significantly better. This random bit mapping

TABLE III  
MAPPING OF BITS  $\mathbf{B} = B_1 B_2 B_3$  TO A STAR-8-QAM SYMBOL  $\mathbf{X}$ .

$\mathbf{B}$	$\mathbf{X}$	$\mathbf{B}$	$\mathbf{X}$
000	$[1 + \sqrt{3}, 1 + \sqrt{3}]$	110	$[-1 - \sqrt{3}, -1 - \sqrt{3}]$
001	$[0, 2]$	111	$[0, -2]$
011	$[-1 - \sqrt{3}, 1 + \sqrt{3}]$	101	$[1 + \sqrt{3}, -1 - \sqrt{3}]$
010	$[-2, 0]$	100	$[2, 0]$

breaks the memory in the practical codes<sup>11</sup> However, random bit mapping is too complex to be practical with today's DSP and is therefore only used for benchmark. Instead the *fixed unstructured bit mapping* can be an interesting practical choice. The curves in the lower part of Fig. 5 show almost the same behavior as for random bit mapping. The curves of the post-SD-FEC BER vs. ASI for uniform signaling with  $\mathbb{M}_{\text{FU}}$  are converged. We examined nine other random seeds for the fixed unstructured bit mapping, and we found no significant difference in the results. While  $\mathbb{M}_{\text{FS1}}$  fails the prediction at  $R_{\text{sdc}} = 1/3$ , it shows smaller required SNR than the others for PAS-64-QAM by 0.1–0.2 dB at  $R_{\text{sdc}} = 5/6$  or 0.3 dB at  $R_{\text{sdc}} = 2/3$  though the small differences are not clearly visible in Figs. 4 and 5. For the all considered bit mappings, ASI is a suitable predictor of the post-FEC BER, especially for PAS.

#### IV. PREDICTION FOR PAS-QAM OVER FIBER-OPTIC CHANNEL

In this section, we discuss the prediction accuracy of the pre-FEC BER in (13), normalized AIR in (14), and ASI in (27). The simulation parameters are listed in Tab. IV. The split-step Fourier method with the Manakov equations was used for simulating the signal propagation over fibers. Lumped optical amplification is used to compensate for the loss of the fiber, and the amplified spontaneous emission noise was loaded per span. In the receiver, the residual chromatic dispersion was compensated in the frequency domain. Adaptive equalization and carrier recovery were performed by fully pilot-aided signal processing [38]. The number of taps in the adaptive equalizer was 21 at 2 samples per symbol, and the adaptation was done by the constant modulus algorithm based on QPSK pilots. The carrier phase at a data symbol was computed by a linear interpolation of the estimated phases from the neighboring two pilot symbols, which were recovered by moving average over the previous and the next pilot symbols. In the soft demapping, the SNR for the auxiliary channel (approximated by the discrete memoryless Gaussian channel) was estimated from the pilot signals. The used FEC was described in Sec. III. The resolution and effective number of bits in digital-to-analog and analog-to-digital conversions were 8 and 6 bits, resp.<sup>12</sup>

To simulate lower post-FEC BER from nonlinearly propagated signals with limited simulation resources, we employed the virtual interleave and scramble technique presented in

<sup>11</sup>The memory break for PAS is limited because the last part of the  $\mathbb{M}_{\text{R}}$  is  $[1, \dots, 1]$ .

<sup>12</sup>The minor differences in the simulation parameters compared to our previous work [14] are the target probability mass function (entropies of a wider range are studied here), the quantization of L-values ( $2^5 \rightarrow 2^{11}$ ), the decoding iterations ( $20 \rightarrow 50$ ), symbol length ( $\sim 2^{15} \rightarrow \sim 2^{16}$ ), number of spans ( $5 \rightarrow 1 \sim 50$ ), and codewords per waveform ( $5 \rightarrow 11$ ).

TABLE IV  
SIMULATION PARAMETERS.

Parameter	Value
Symbol rate	32 Gsymbol/s
Spectral shaping	root-raised cosine, 1% roll-off
Channel spacing	$32 \times 1.01$ GHz
Number of channels	7
Launch power	$[-7.5, +4.5]$ dBm/channel
Fiber attenuation	0.2 dB/km
Chromatic dispersion	17 ps/nm/km
Nonlinear coefficient	$1.2 \text{ W}^{-1}\text{km}^{-1}$
Span length	100 km
Number of spans	[1, 50] (PAS-64-QAMs) [1, 30] Uniform 64-QAM
Noise figure of amplifier	5 dB
Laser linewidth	100 kHz
Pilot insertion ratio	4%

[30], [39]–[41]. Then, totally more than 500 codewords were simulated to obtain each point. The bit mappings  $\mathbb{M}_{\text{FS1}}$  and  $\mathbb{M}_{\text{FU}}$  were examined. Each codeword was further interleaved over time, both polarizations, and both quadratures.

Fig. 6 shows ASI vs. number of spans for (a) uniform 64-QAM, (b) PAS-64-QAM (i), (c) PAS-64-QAM (ii), and (d) PAS-64-QAM (iii). FEC decoding with an SD-FEC code rate  $R_{\text{sdc}}$  2/3, 3/4, 5/6, or 9/10 was performed for ASI = [0.66, 0.74], [0.74, 0.82], [0.82, 0.88], or [0.88, 0.94]. To include both linear and nonlinear cases for each shaping parameter and each code rate, we studied 4.5 dBm/channel for PAS-64-QAM (i). Except for that, the maximum launch power was 3 dBm/channel.

For a given combination of number of spans and launch power, we can choose suitable shaping and FEC parameters from Fig. 6. For example, at 25 spans and 0 dBm/channel, PAS-64-QAM (ii) with  $R_{\text{sdc}} = 9/10$  or PAS-64-QAM (iii) with  $R_{\text{sdc}} = 5/6$  would be good candidates for reliable and spectrally efficient communication.

Figs. 7 and 8 show post-SD-FEC BER as a function of the various metrics (pre-FEC BER, normalized AIR, ASI). Open markers show the low nonlinearity cases with launch powers of  $[-7.5, -3]$  dBm/channel, and filled markers those with high nonlinearity,  $[-1.5, +4.5]$  dBm/channel. For reference, simulation results over the Gaussian channel are shown by solid lines. The vertical dashed lines in Figs. 7(a), 7(c), 8(a), and 8(c) show the peak-to-peak variation of the curves in the nonlinear transmission cases. At the same FEC code rate, shaping parameter, and a given post-FEC BER, relatively larger pre-FEC BER or almost the same ASI is required in the fiber-optic channel compared with the Gaussian channel. Normalized AIR does not work, and in particular low-entropy cases (stronger shaping) are problematic. The convergence of the curves with  $\mathbb{M}_{\text{FS1}}$  is worse than that with  $\mathbb{M}_{\text{FU}}$ . The prediction errors are summarized in Tab. V. The errors at a given  $R_{\text{sdc}}$  are quantified both horizontally ( $\Delta\text{Metric}$ ) and vertically ( $\Delta\text{BER}_{\text{post-SD}}$ ) around the post-SD-FEC BER of  $5 \times 10^{-5}$ , which corresponds to a certain HD-FEC limit [36]. The prediction error  $\Delta\text{BER}_{\text{pre}}$  appears to be smaller than  $\Delta\text{ASI}$ , but since its variation is around a much smaller metric value, the relative error is larger. This observation is consistent with  $\Delta\text{BER}_{\text{post-SD}}$ , cf. [13], [14], whose variation with ASI is

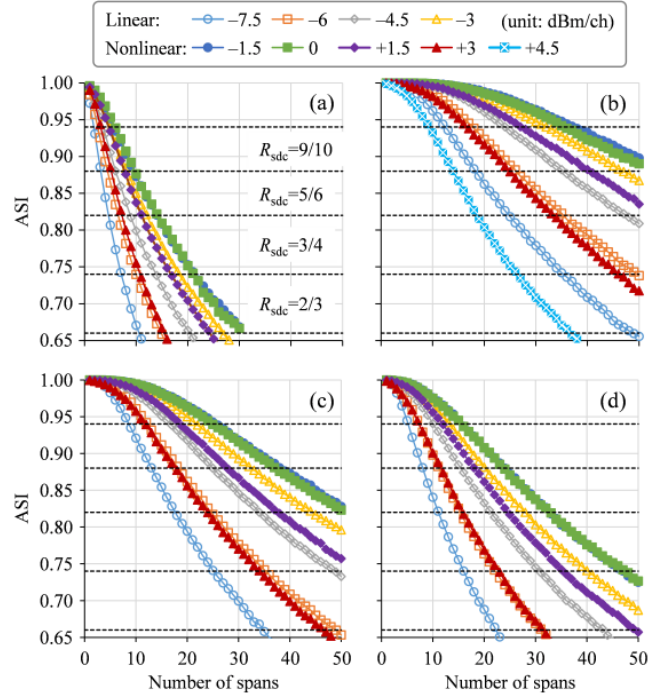


Fig. 6. ASI vs. number of spans for (a) uniform 64-QAM, (b) PAS-64-QAM (i), (c) PAS-64-QAM (ii), and (d) PAS-64-QAM (iii).

TABLE V  
SIMULATED PREDICTION ERRORS OF POST-SD-FEC BER OVER THE FIBER-OPTIC CHANNELS.

Bit mapping: $\mathbb{M}_{\text{FS1}}$					
$R_{\text{sdc}}$	$\Delta\text{Metric}$		$\Delta\text{BER}_{\text{post-SD}}$		
	$\text{BER}_{\text{pre}}$	ASI	$\text{BER}_{\text{pre}}$	ASI	
2/3	$2.9 \times 10^{-3}$	$3.5 \times 10^{-3}$	$4.4 \times 10^4$	$5.6 \times 10^1$	
3/4	$2.5 \times 10^{-3}$	$5.0 \times 10^{-3}$	$3.2 \times 10^4$	$3.2 \times 10^2$	
5/6	$1.9 \times 10^{-3}$	$3.0 \times 10^{-3}$	$2.6 \times 10^3$	$6.3 \times 10^1$	
9/10	$1.9 \times 10^{-3}$	$4.0 \times 10^{-3}$	$6.3 \times 10^3$	$1.6 \times 10^3$	
Bit mapping: $\mathbb{M}_{\text{FU}}$					
$R_{\text{sdc}}$	$\Delta\text{Metric}$		$\Delta\text{BER}_{\text{post-SD}}$		
	$\text{BER}_{\text{pre}}$	ASI	$\text{BER}_{\text{pre}}$	ASI	
2/3	$9.2 \times 10^{-3}$	$1.8 \times 10^{-2}$	$9.1 \times 10^{11}$	$1.6 \times 10^7$	
3/4	$5.0 \times 10^{-3}$	$8.0 \times 10^{-3}$	$1.0 \times 10^8$	$1.0 \times 10^4$	
5/6	$4.9 \times 10^{-3}$	$1.1 \times 10^{-2}$	$2.0 \times 10^9$	$1.4 \times 10^7$	
9/10	$3.0 \times 10^{-3}$	$6.0 \times 10^{-3}$	$1.0 \times 10^6$	$6.3 \times 10^4$	

between 4 and 790 times less than the corresponding variation with pre-FEC BER for  $\mathbb{M}_{\text{FS1}}$ , and between 16 and 57,000 times less for  $\mathbb{M}_{\text{FU}}$ .

From the Gaussian channel simulations over a wide range of spectral efficiencies in Figs. 4 and 5, the ASI predicts post-FEC BER better than pre-FEC BER in the case of *fixed unstructured bit mapping*  $\mathbb{M}_{\text{FU}}$ . On the other hand, as explained in Sec. III-B, last paragraph,  $\mathbb{M}_{\text{FS1}}$  gives a slightly smaller ASI (smaller SNR) at a FEC threshold than  $\mathbb{M}_{\text{FU}}$  for PAS-64-QAMs (and also for uniform 64-QAM). In the transmission simulation in Figs. 7 and 8 with a limited range of spectral efficiencies,  $\mathbb{M}_{\text{FS1}}$  shows not only better performance at a FEC threshold but also better accuracy of post-FEC BER prediction than  $\mathbb{M}_{\text{FU}}$  under the (admittedly limited) examined modulation and FEC cases.

Here we can suggest an open problem for possible future research. We start with finding find a good (nearly optimum)



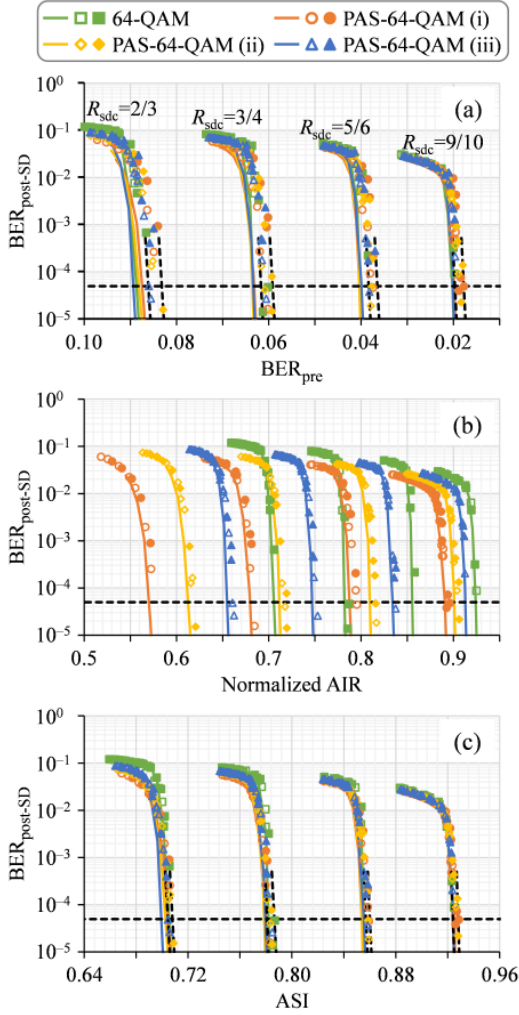


Fig. 7. Post-SD-FEC BER as a function of (a) pre-FEC BER, (b) normalized AIR, or (c) ASI on fiber-optic channel with bit mapping  $\mathbb{M}_{FS1}$ .

bit mapping  $\mathbb{M}_{opt}$ , which can be different for each combination of modulation, shaping, and FEC code rate. Then, we quantify numerically the relation between the ASI and post-FEC BER. At least the required SNR performance will be nearly optimum for each signal. Here it would be very interesting to study how the prediction accuracy of also the post-FEC BER becomes. Judging from the results in this section, the post-FEC prediction accuracy might be good as well.

## V. CONCLUSIONS

We showed theoretically the equivalence of NGMI and ASI for matched decoding. We then examined, for approximately matched decoding, where  $ASI \approx NGMI$ , the ASI and NGMI as metrics to predict the post-SD-FEC BER under various combinations of modulation, shaping, and code rates. The limitation of the metric is the post-SD-FEC BER dependence on the code structure. In the case of high code rates, e.g.,  $\geq 2/3$ , there are less issues, and even the pre-FEC BER would work, e.g., for in-service performance monitoring, if the FEC limit difference is taken into account. The post-SD-FEC BER in the case of lower code rates depends on the code structure and the bit mapping more significantly. Thus, the ASI and

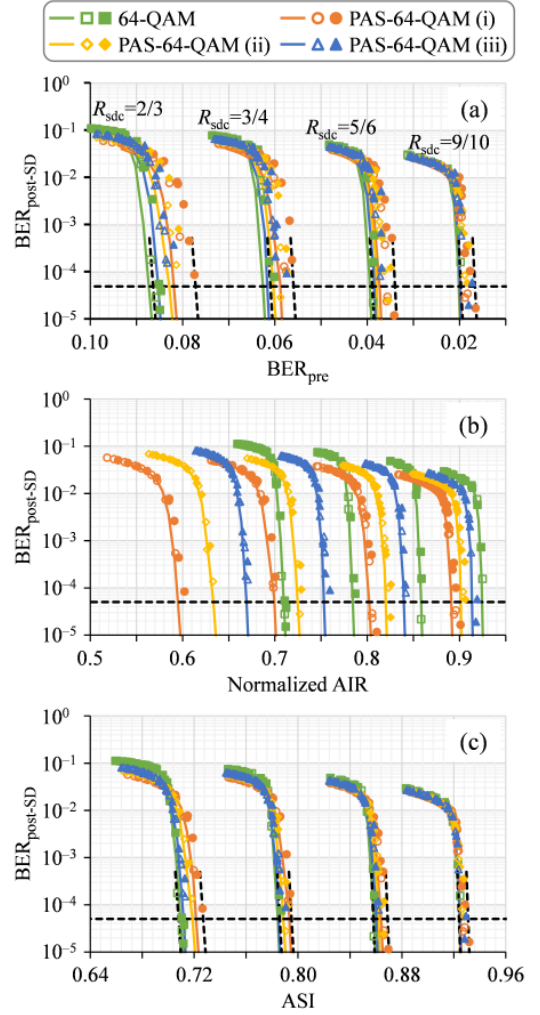


Fig. 8. Post-SD-FEC BER as a function of (a) pre-FEC BER, (b) normalized AIR, or (c) ASI on fiber-optic channel with bit mapping  $\mathbb{M}_{FU}$ .

NGMI, which cannot take code structure into account, do not always predict the post-SD-FEC BER accurately. However, when we break the code structure by a random bit mapping, or even fixed unstructured bit mapping, the prediction accuracy improves significantly. The prediction by the pre-FEC BER is significantly worse at low code rates even if we break the code structure. The observation for the Gaussian channel is useful for the fiber-optic channel with nonlinearity as well, though the prediction errors become larger for limited data sizes or non-Gaussian-channel signal degradations.

## ACKNOWLEDGMENTS

We thank Koji Igarashi of Osaka University for fruitful discussions about performance metrics.

## PROOF OF THEOREM 1

The  $I_{q,s=1}^{\text{gmi}}(\mathbf{B}; \mathbf{Y})$  is reformulated from (6) and (7), as well as the reformulation in [8, Th. 4.11],

$$I_{q,s=1}^{\text{gmi}}(\mathbf{B}; \mathbf{Y}) = \mathbb{E}_{\mathbf{B}, \mathbf{Y}} \left[ \log_2 \frac{\prod_{i=1}^m P_{B_i}(B)}{\sum_{\mathbf{b} \in \mathbb{B}^m} \prod_{i=1}^m P_{B_i}(b) q_{\mathbf{Y}|B_i}(\mathbf{Y} | B)} \right] \quad (28)$$

$$= \mathbb{E}_{\mathbf{B}, \mathbf{Y}} [\log_2 \prod_{i=1}^m P_{B_i}(B)] - \mathbb{E}_{\mathbf{B}, \mathbf{Y}} [\log_2 P_{\mathbf{B}}(\mathbf{B})] + \mathbb{E}_{\mathbf{B}, \mathbf{Y}} \left[ \log_2 \frac{\prod_{i=1}^m q_{\mathbf{Y}|B_i}(\mathbf{Y} | B)}{\sum_{\mathbf{b} \in \mathbb{B}^m} \prod_{i=1}^m P_{B_i}(b) q_{\mathbf{Y}|B_i}(\mathbf{Y} | b)} \right] \quad (29)$$

$$= \sum_{i=1}^m \mathbb{E}_{\mathbf{B}} [\log_2 P_{B_i}(B)] - \mathbb{E}_{\mathbf{B}} [\log_2 P_{\mathbf{B}}(\mathbf{B})] + \mathbb{E}_{\mathbf{B}, \mathbf{Y}} \left[ \log_2 \frac{\prod_{i=1}^m q_{\mathbf{Y}|B_i}(\mathbf{Y} | B)}{\prod_{i=1}^m \sum_{b \in \mathbb{B}} P_{B_i}(b) q_{\mathbf{Y}|B_i}(\mathbf{Y} | b)} \right] \quad (30)$$

$$= - \sum_{i=1}^m \mathbb{H}(B_i) + \mathbb{H}(\mathbf{B}) + \sum_{i=1}^m I_{q_i, s=1}^{\text{gmi}}(B_i; \mathbf{Y}), \quad (31)$$

where the third term is shown in [8, Eq. (4.47)], i.e.,

$$I_{q_i, s}^{\text{gmi}}(B_i; \mathbf{Y}) = \mathbb{E}_{B_i, \mathbf{Y}} \left[ \log_2 \frac{q_{\mathbf{Y}|B_i}(\mathbf{Y} | B)^s}{\sum_{b \in \mathbb{B}} P_{B_i}(b) q_{\mathbf{Y}|B_i}(\mathbf{Y} | b)^s} \right]. \quad (32)$$

By employing [8, Th. 4.20], (32) is reformulated to

$$I_{q_i, s=1}^{\text{gmi}}(B_i; \mathbf{Y}) = \mathbb{H}(B_i) - \sum_{b \in \mathbb{B}} P_{B_i}(b) \cdot \mathbb{E}_{L_i | B_i=b} [\log_2(1 + \exp(-(-1)^b L_i))]. \quad (33)$$

Applying (33) to (31), we obtain

$$I_{q, s=1}^{\text{gmi}}(\mathbf{B}; \mathbf{Y}) = \mathbb{H}(\mathbf{B}) - \sum_{i=1}^m \sum_{b \in \mathbb{B}} P_{B_i}(b) \cdot \mathbb{E}_{L_i | B_i=b} [\log_2(1 + \exp(-(-1)^b \cdot l))]. \quad (34)$$

A reformulated description of ASI in (18) is

$$\text{ASI} = \mathbb{E}_{L_a} \left[ \log_2 \frac{2p_{L_a}(l)}{p_{|L_a|}(|l|)} \right], \quad (35)$$

$$= - \mathbb{E}_{L_a} \left[ \log_2 \left( 1 + \frac{p_{L_a}(-l)}{p_{L_a}(l)} \right) \right]. \quad (36)$$

By considering [8, Eq. (3.67)], one can derive

$$\text{ASI} = 1 - \mathbb{E}_{L_a} [\log_2(1 + \exp(-l))]. \quad (37)$$

By introducing asymmetric L-value per bit tributary  $L_{a,i} = (-1)^{B_i} L_i$ , and  $(1/m) \sum_{i=1}^m p_{L_{a,i}}(l) = p_{L_a}(l)$ ,

$$\text{ASI} = 1 - \frac{1}{m} \sum_{i=1}^m \mathbb{E}_{L_{a,i}} [\log_2(1 + \exp(-l))] \quad (38)$$

$$= 1 - \frac{1}{m} \sum_{i=1}^m \sum_{b \in \{0,1\}} P_{B_i}(b) \cdot \mathbb{E}_{L_i | B_i=b} [\log_2(1 + \exp(-(-1)^b \cdot l))]. \quad (39)$$

According to (34) and (39), (24) is derived.

## REFERENCES

- [1] E. Agrell and M. Secondini, "Information-theoretic tools for optical communications engineers," in *Proc. IEEE Phot. Conf. (IPC)*, Reston, VA, Sep.–Oct. 2018.
- [2] J. Cho, S. L. I. Olsson, S. Chandrasekhar, and P. Winzer, "Information rate of probabilistically shaped QAM with non-ideal forward error correction," in *Proc. Eur. Conf. on Opt. Comm. (ECOC)*, Rome, Italy, Sep. 2018, Paper Th.1.H.5.
- [3] J. Cho and P. J. Winzer, "Probabilistic constellation shaping for optical fiber communications," *IEEE/OSA J. Lightw. Technol.*, vol. 37, no. 6, pp. 1590–1607, Mar. 2019.
- [4] O. Vassilieva, I. Kim, and T. Ikeuchi, "On the fairness of the performance evaluation of probabilistically shaped QAM," in *Proc. Eur. Conf. Opt. Commun. (ECOC)*, Dublin, Ireland, Sep. 2019, Paper Th.2.B.2.
- [5] E. Zehavi, "8-PSK trellis codes for a Rayleigh channel," *IEEE Trans. Commun.*, vol. 40, no. 3, pp. 873–884, May 1992.
- [6] G. Caire, G. Taricco, and E. Biglieri, "Bit-interleaved coded modulation," *IEEE Trans. Inf. Theory*, vol. 44, no. 3, pp. 927–946, May 1998.
- [7] A. Guillén i Fàbregas, A. Martinez, and G. Caire, "Bit-interleaved coded modulation," *Found. Trends Commun. Inf. Theory*, vol. 5, nos. 1/2, pp. 1–153, 2008.
- [8] L. Szczecinski and A. Alvarado, *Bit-Interleaved Coded Modulation: Fundamentals, Analysis, and Design*. Chichester, UK, John Wiley & Sons, 2015.
- [9] G. Böcherer, F. Steiner, and P. Schulte, "Bandwidth efficient and rate-matched low-density parity-check coded modulation," *IEEE Trans. Commun.*, vol. 63, no. 12, pp. 4651–4665, Dec. 2015.
- [10] G. Böcherer, P. Schulte, and F. Steiner, "Probabilistic shaping and forward error correction for fiber-optic communication systems," *IEEE/OSA J. Lightw. Technol.*, vol. 37, no. 2, pp. 230–244, Jan. 2019.
- [11] A. Alvarado, E. Agrell, D. Lavery, R. Maher, and P. Bayvel, "Replacing the soft-decision FEC limit paradigm in the design of optical communication systems," *IEEE/OSA J. Lightw. Technol.*, vol. 33, no. 20, pp. 4338–4352, Oct. 2015.
- [12] J. Cho, L. Schmalen, and P. Winzer, "Normalized generalized mutual information as a forward error correction threshold for probabilistically shaped QAM," in *Proc. Eur. Conf. Opt. Commun. (ECOC)*, Göteborg, Sweden, Sep. 2017, Paper M.2.D.2.
- [13] T. Yoshida, M. Karlsson, and E. Agrell, "Performance metrics for systems with soft-decision FEC and probabilistic shaping," *IEEE Photon. Technol. Lett.*, vol. 29, no. 23, pp. 2111–2114, Dec. 2017.
- [14] T. Yoshida, M. Karlsson, and E. Agrell, "Post-FEC BER Prediction Accuracy for Probabilistically Shaped Signaling in Fiber-Optic Communications," in *Proc. Eur. Conf. on Opt. Comm. (ECOC)*, Göteborg, Sweden, Sep. 2017, Paper Mo.2.D.3.
- [15] R. Maher, K. Croussore, M. Lauermann, R. Going, and J. Rahn, "Constellation shaped 66 Gbd DP-1024QAM transceiver with 400 km transmission over standard SMF," in *Proc. Eur. Conf. on Opt. Comm. (ECOC)*, Göteborg, Sweden, Sep. 2017, Paper Th.PDP.B.2.
- [16] H.-C. Chien, J. Yu, B. Zhu, J. Shi, Y. Cai, X. Xiao, Y. Xia, X. Wei, and Y. Chen, "Probabilistically shaped DP-64QAM coherent optics at 105 Gbd achieving 900 Gbps net bit rate per carrier over 800 km transmission," in *Proc. Eur. Conf. on Opt. Comm. (ECOC)*, Rome, Italy, Sep. 2018, Paper Th.PDP.B.2.
- [17] G. Böcherer, "Achievable rates for probabilistic shaping," [Online]. Available: [www.arxiv.org/pdf/1707.01134v5](http://www.arxiv.org/pdf/1707.01134v5)
- [18] T. Yoshida, M. Karlsson, and E. Agrell, "Technologies toward implementation of probabilistic constellation shaping," in *Proc. Eur. Conf. on Opt. Comm. (ECOC)*, Rome, Italy, Sep. 2018, Paper Th.1.H.1.
- [19] T. Yoshida, M. Karlsson, and E. Agrell, "Hierarchical distribution matching for probabilistically shaped coded modulation," *IEEE/OSA J. Lightw. Technol.*, vol. 37, no. 6, pp. 1579–1589, Mar. 2019.
- [20] S. Zhang, F. Yaman, E. Mateo, I. B. Djordjevic, K. Nakamura, T. Inoue, Y. Inada, "On the performance metric and design of non-uniformly shaped constellation," in *Proc. Opt. Fiber Commun. Conf. (OFC)*, San Diego, CA, USA, Mar. 2019, Paper W1D.7.
- [21] C. Häger, A. Graell i Amat, F. Brännström, A. Alvarado, and E. Agrell, "Improving soft FEC performance for higher-order modulations via optimized bit channel mappings," *Opt. Expr.*, vol. 22, no. 12, pp. 14544–14558, May 2014.
- [22] A. Amari, S. Goossens, Y. C. Gültekin, O. Vassilieva, I. Kim, T. Ikeuchi, C. Okonkwo, F. M. J. Willems, and A. Alvarado, "Introducing enumerative sphere shaping for optical communication systems with short blocklengths," [Online]. Available: <https://arxiv.org/pdf/1904.06601v3>
- [23] P. Schulte and G. Böcherer, "Constant composition distribution matching," *IEEE Trans. Inf. Theory*, vol. 62, no. 1, pp. 430–434, Jan. 2016.
- [24] T. Fehenberger, D. S. Millar, T. Koike-Akino, K. Kojima, and K. Parsons, "Multiset-partition distribution matching," *IEEE Trans. Commun.*, vol. 67, no. 3, pp. 1885–1893, Mar. 2019.

- [25] J. Cho and P. Winzer, "Multi-rate prefix-free code distribution matching," in *Proc. Opt. Fib. Commun. Conf. (OFC)*, San Diego, CA, USA, Mar. 2019, Paper M4B.7.
- [26] Y. C. Gültekin, F. M. J. Willems, W. J. Houtum, and S. Şerbetli, "Constellation shaping for IEEE 802.11," in *Proc. IEEE 28th Annu. Int. Symp. Pers., Indoor, Mobile Radio Commun.*, Montreal, QC, Canada, Oct. 2017.
- [27] A. Alvarado, L. Szczecinski, T. Fehenberger, M. Paskov, and P. Bayvel, "Improved soft-decision forward error correction via post-processing of mismatched log-likelihood ratios," in *Proc. Eur. Conf. Opt. Commun. (ECOC)*, Düsseldorf, Germany, Sep. 2016, Paper W.2.C.5.
- [28] T. T. Nguyen and L. Lampe, "Bit-interleaved coded modulation with mismatched decoding metrics," *IEEE Trans. Commun.*, vol. 59, no. 2, pp. 437–447, Feb. 2011.
- [29] L. Szczecinski, "Correction of Mismatched L-values in BICM Receivers," *IEEE Trans. Commun.*, vol. 60, no. 11, pp. 3198–3208, Nov. 2012.
- [30] F. Buchali, F. Steiner, G. Böcherer, L. Schmalen, P. Schulte, and W. Idler, "Rate adaptation and reach increase by probabilistically shaped 64-QAM: an experimental demonstration," *IEEE/OSA J. Lightw. Technol.*, vol. 34, no. 7, pp. 1599–1609, Apr. 2016.
- [31] A. Alvarado, E. Agrell, D. Lavery, and P. Bayvel, "LDPC codes for optical channels: Is the "FEC Limit" a good predictor of post-FEC BER?," in *Proc. Opt. Fiber Commun. Conf. (OFC)*, Los Angeles, CA, USA, Mar. 2015, Paper Th3E.5.
- [32] A. Alvarado, T. Fehenberger, B. Chen, F. M. J. Willems, "Achievable information rates for fiber optics: applications and computations," *IEEE/OSA J. Lightw. Technol.*, vol. 36, no. 2, pp. 424–439, Jan. 2018.
- [33] M. Ivanov, C. Häger, F. Brännström, A. Graell i Amat, A. Alvarado, and E. Agrell, "On the information loss of the max-log approximation in BICM systems," *IEEE Trans. Inf. Theory*, vol. 62, no. 6, pp. 3011–3025, June 2016.
- [34] T. Koike-Akino, K. Kojima, D. S. Millar, K. Parsons, T. Yoshida, and T. Sugihara, "Pareto optimization of adaptive modulation and coding set in nonlinear fiber-optic systems," *IEEE/OSA J. Lightw. Technol.*, vol. 35, no. 4, pp. 1041–1049, Feb. 2017.
- [35] European Telecommunications Standards Institute, "Second generation framing structure, channel coding and modulation systems for broadcasting, interactive services, news gathering and other broadband satellite applications; Part 1 (DVB-S2)," ETSI Standard EN 302 307-1 V1.4.1, Nov. 2014. [Online]. Available: [www.dvb.org/standards](http://www.dvb.org/standards)
- [36] D. S. Millar, R. Maher, D. Lavery, T. Koike-Akino, M. Pajovic, A. Alvarado, M. Paskov, K. Kojima, K. Parsons, B. C. Thomsen, S. Savory, and P. Bayvel, "Detection of a 1 Tb/s superchannel with a single coherent receiver," in *Proc. Eur. Conf. Opt. Commun. (ECOC)*, Valencia, Spain, Sep. 2015, Paper Mo.3.3.1.
- [37] S. ten Brink, G. Kramer, and A. Ashikhmin, "Design of low-density parity-check codes for modulation and detection," *IEEE Trans. Commun.*, vol. 52, no. 4, pp. 670–678, Apr. 2004.
- [38] M. Mazur, J. Schröder, A. Lorences-Riesgo, T. Yoshida, M. Karlsson, and P. A. Andrekson, "Overhead-optimization of pilot-based digital signal processing for flexible high spectral efficiency transmission," *OSA Opt. Express*, vol. 27, no. 17, pp. 24654–24669, Aug. 2019.
- [39] L. Schmalen, F. Buchali, A. Leven, and S. ten Brink, "A generic tool for assessing the soft-FEC performance in optical transmission experiments," *IEEE Photon. Technol. Lett.*, vol. 24, no. 1, pp. 40–42, Jan. 2012.
- [40] N. Stojanovic, Y. Zhao, D. Chang, Z. Xiao, and F. Yu, "Reusing common uncoded experimental data in performance estimation of different FEC codes," *IEEE Photon. Technol. Lett.*, vol. 25, no. 24, pp. 2494–2497, Dec. 2013.
- [41] T. Yoshida, M. Karlsson, and E. Agrell, "Efficient offline evaluation of FEC codes based on captured data with probabilistic shaping," in *Proc. Opt. Fiber Commun. Conf. (OFC)*, San Diego, CA, USA, Mar. 2018, Paper M4E.5.